Numerical Analysis and Computer Simulation of Magnetostatic Wave Propagation in a YIG-Loaded Waveguide

Matthew M. Radmanesh, *Member, IEEE*, Chiao-Min Chu, and George I. Haddad

Abstract—**Magnetostatic Wave (MSW) propagation in a finite-width ferrite slab placed inside and along a rectangular waveguide is investigated theoretically and numerically. Using the integral equation method, the general solution to the problem of wave propagation has been derived for the first time here in this paper. Thin-slab approximation made the derived solution more tractable and provided the dispersion relations in terms of an infinite determinant. From the presented results, it can be concluded that in order to obtain high value of group time delay over a large bandwidth thin, narrow slabs placed in the center of the guide must be used. On the other hand, to maximize the device bandwidth, thin slabs placed at the top or bottom of the guide are most appropriate.**

I. Introduction

ANALYSIS of magnetostatic wave (MSW) propagation in a ferrite material in a normally magnetized structure bound by metal surfaces has been extensively reported in literature [1]–[5]. MSW propagation in a ferrite slab completely filling a waveguide has also been analyzed and documented [6]. Recently the analysis of magnetostatic waves in a YIG-loaded waveguide was reported [7], [8]. The mathematical analysis carried out by these recent investigations were based on a parallel magnetic bias field which led to the propagation of magnetostatic surface waves (MSSW). These waves are highly nonreciprocal with respect to the direction of propagation and unsymmetrical with respect to the slab position in the waveguide. Koshiba *et al.* [9], [10] provided a unified numerical approach based on the finite-element method where both cases of parallel and normal magnetization were studied. However the problem of magnetostatic wave propagation in a YIG slab enclosed in a waveguide with normal magnetic bias field (Magnetostatic Forward Volume Waves, MSFVW) has not been approached using the integral equation method (see Fig. 1). A brief account of this method was presented in the 1988 IEEE-MTT's Digest [11]. In this Digest article, the problem of MSW propagation in a normally magnetized YIG-loaded waveguide was sketchily outlined and yet no attempt to solve the problem or provide supporting formulation or reasonings was undertaken and thus a very scanty and ambiguous view of the resolution of the problem was presented. The present work, however, attempts to clear the way and present a highly coherent and understandable view of the MSW propagation and all of its inherent complexities.

Manuscript received Apr. 23, 1992; revised Apr. 23, 1992. This work was supported in part by the Air Force Systems Command, Avionics Laboratory, Wright-Patterson Air Force Base, Ohio under Contract no. F-33615-81-8-1429.

M. M. Radmanesh is with the Electrical and Computer Engineering Department, California State University, Northridge, Northridge, CA 91330.

C. M. Chu and G. I. Haddad are with the Electrical Engineering and Computer Science Department, The University of Michigan 48109-2122.

IEEE Log Number 9204026.

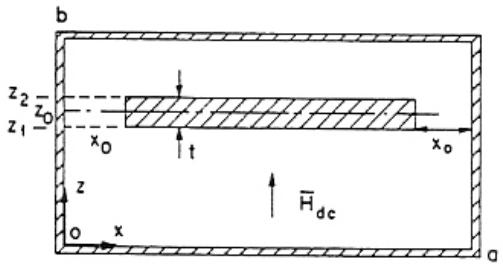

Fig. 1. Device configuration for H_{dc} normal to the YIG slab.

In this paper, the analysis of magnetostatic waves in a waveguide structure with the normal magnetic field as shown in Fig. 1 is carried out in detail. For this configuration, when the gap length (x_0) is zero, the problem can be treated as a boundary value problem and conventional mode analysis technique can be employed effectively to solve for the dispersion characteristics for the different modes of propagation [12].

However, when x_0 is nonzero, the mode analysis techniques appear to be fruitless and the integral equation method seems to be one of the most effective method in this case and provides the desired dispersion relations.

Section II briefly describes the underlying Magnetostatic EM Fields. The integral equation method and the general solution for the scalar magnetic potential function in terms of an integrodifferential equation is presented in Section III. In Section IV, using thin slab approximation an approximate solution is obtained. Numerical analysis and results of computer simulation for the first-order mode are presented in Section V. Summary and conclusions along with some final discussions follow in Section VI.

II. Magnetostatic EM Fields

In this Section, the mathematical foundation for magnetostatic wave propagation in unbounded and bounded ferrite media is introduced and the governing equations are derived. Magnetostatic waves have wavelengths much greater than the

lattice spacing, therefore it is appropriate to use classical theory rather than quantum theory, thus the small signal theory of a lossless ferrite is based on the Maxwell's equations.

The tensor permeability of a ferrite is derived using Newton's equation of motion where the exchange and core losses are neglected. Utilizing this permeability tensor, the wave propagation in unbounded ferrites leads to three regions of interest in the frequency-wave number (ω-k) plane. It is seen that magnetostatic wave propagation is possible only in a limited range of wavelengths [13]. In this range of wavelengths, the electric field is negligibly small compared with the magnetic field and can be neglected. Thus Maxwell's equations can be simplified and the magnetic field can be derived directly from a scalar potential function. When this approximation is used the governing partial differential equations inside as well as outside the YIG slab can be derived as follows:

$$\nabla \times \overline{h} = 0 \rightarrow \overline{h} = \nabla \Psi(x, y, z)$$

$$\nabla \cdot \overline{b} = 0 \tag{1}$$

$$\nabla \cdot \left[\overline{\overline{\mu}} \cdot \nabla \Psi(x, y, z)\right] = 0. \tag{2}$$

Where $\overline{\overline{\mu}}$ is the permeability tensor, $\overline{h}$ is the small signal magnetic field intensity and $\Psi(x, y, z)$ is the scalar magnetic potential function. It should be noted that in the air region outside the YIG slab, (2) is valid except for $\overline{\overline{\mu}}$ which should be replaced by scalar μ_0, the permeability of free space.

Utilizing these equations, Wave Propagation in a YIG loaded rectangular waveguide under the magnetostatic approximation can now be approached and a set of boundary conditions which must be satisfied at the metal surfaces can be derived. It is further assumed that the transverse dimensions of the waveguide are small compared to the electromagnetic wavelengths and thus the waveguide's electromagnetic modes are either cut-off or leaky waves.

III. The Integral Equation Method

The analysis of the magnetostatic wave propagation in a finite-width YIG slab appears to be feasible by the utilization of the integral equation method. To be able to use this method effectively, it is best to deduce the integral equation in the steps as outlined in the following. The time dependence is of the form $e^{j\omega t}$, (ω being the angular frequency) and is omitted in all of the following expressions. The integral equation is developed in the following systematic way:

1. the magnetostatic wave propagation is assumed to be in the y-direction and thus of the form e^{-jKy} where K is the wave number. In this manner, the y-variation of all functions involved in this study is of the form e^{-jKy}, which can be omitted since it is a common factor in all of the subsequent formulations.
2. An unknown scalar magnetic potential function inside the ferrite slab is assumed. The potential function for all the points inside the slab is denoted by $\Psi(x, y, z)$. Based on $\Psi(x, y, z)$, fictitious magnetic sources can be obtained. The scalar magnetic potential function $\Psi(x, y, z)$ inside the YIG region can be written as:

$$\Psi(x, y, z) = \Phi(x, z)e^{-jKy}. \tag{3}$$

Then, except for the common factor e^{-jKy}, the small signal magnetic field intensity, the magnetic flux density, and the magnetization intensity vectors in the YIG region designated by $\overline{h}, \overline{b}$ and $\overline{m}$ respectively are given by

$$\overline{h} = \nabla\phi - jK\phi\hat{y} \tag{4}$$

$$\overline{b} = \mu_0[\overline{\overline{\mu}}_r] \cdot \overline{h} \tag{5}$$

$$\overline{m} = \left([\overline{\overline{\mu}}_r] - [\overline{\overline{I}}]\right) \cdot \overline{h} \tag{6}$$

where $\hat{y}$ is a unit vector in the y-direction, $[\overline{\overline{I}}]$ is the identity tensor and $[\overline{\overline{\mu}}_r]$ is the relative permeability tensor [12].

3. From the small signal magnetization intensity ($\overline{m}$) given by (6), the magnetic sources can be determined. The total magnetic charge density consists of two portions: a) the magnetic volume charge density (ρ_v) and b) the magnetic surface charge density (ρ_s). These magnetic sources can be expressed as

$$\rho_v = -\nabla \cdot (\overline{m}e^{-jKy}) \tag{7}$$

$$\rho_v = \overline{m} \cdot \hat{n} \tag{8}$$

where $\hat{n}$ is a unit vector normal to the slab surface. Substituting (6) in (7) and (8) and upon further simplifications, ρ_v and ρ_s are finally given by

$$\rho_v(x, z) = \frac{\mu - 1}{\mu}\Phi_{zz}(x, z) \tag{9}$$

$$\rho_s(x_0, z) = -(\mu - 1)\Phi_x(x_0, z) - K_1 K\Phi(x_0, z) \tag{10a}$$

$$\rho_s(a - x_0, z) = (\mu - 1)\Phi_x(a - x_0, z) + K_1 K\Phi(a - x_0, z) \tag{10b}$$

where μ and K_1 are the diagonal and off-diagonal elements of the permeablity tensor, respectively [12], and Φ_{zz} is the second-order derivative of Φ with respect to z and Φ_x is the first-order derivative with respect to x. From (10), it can be seen that unlike parallel magnetization case [8], the surface charges at $z = z_1$ or z_2 are absent and the only existing surface charges are at $x = x_0$ and $x = a - x_0$. It will be seen that this difference in the charge arrangement and mathematical form for the two cases will lead to different formulations entirely.

4. The Green's function $G(x, z)e^{-jKy}$, for a magnetic line source located at (x', z') along and inside a waveguide, is given by

$$G(x, x', z, z') = \sum_{n=0}^{\infty} A_n \cos(n\pi x'/a)\cos(n\pi x/a) \cdot \operatorname{Cosh}\gamma_n'(b - z')\operatorname{Cosh}\gamma_n' z \tag{11a}$$

for $z < z'$, and by:

$$G(x, x', z, z') = \sum_{n=0}^{\infty} A_n \cos(n\pi x'/a)\cos(n\pi x/a) \cdot \operatorname{Cosh}\gamma_n'(b - z)\operatorname{Cosh}\gamma_n' z' \tag{11b}$$

for $z > z'$: where

$$A_n = \frac{-2}{\gamma_n' a(1+\delta_{on})\sinh \gamma_n' b}$$
$$\gamma_n' = [K^2 + (n\pi/a)^2]^{1/2}$$

and δ_{on} is the Kronecker delta function.

5. At this point in the development of the formulation, an important distinction for the magnetic potential *inside the waveguide* and *inside the ferrite slab* is made as follows:
   a. $\Phi^{\dagger}(x,z)$ is the scalar magnetic potential function inside the waveguide (including the ferrite slab) and is defined for $0 \le x \le a$ and $0 \le z \le b$.
   b. $\Phi(x,z)$ is a scalar magnetic potential function inside the ferrite slab and is defined for $x_o \le x \le a - x_o$ and $z_1 \le z \le z_2$.

   With this convention, the developed formulations which will appear later in this work can easily be assimilated.
6. Considering a uniform waveguide cross section and wave propagation in one unit length, and by means of the magnetic sources (9), (10) and the suitable Green's function (11), an integral expression for the potential function $\Phi^{\dagger}(x,z)$ everywhere inside the waveguide (including the ferrite) can be written as:

$$\Phi^{\dagger}(x,z) = \iint_{\text{YIG area}} \rho_v(x',z')G(x,x',z,z')dx'dz' + \int_{\text{YIG sides}} \rho_s(x'z')G(x,x',z,z')dz' \quad (12)$$

Using (9), (10), and (11) and considering only the points located inside the ferrite slab, from (12) an integro-differential equation in terms of $\Phi(x,z)$ is obtained:

$$\begin{aligned}\Phi(x,z) &= \int_{x_o}^{a-x_o}\int_{z_1}^{z_2}\left[\left(\frac{\mu-1}{\mu}\right)\Phi_{zz}(x',z')\right]G(x,x',z,z')dz'dx' \\ &\quad - \int_{z_1}^{z_2}\left[(\mu-1)\Phi_x(x_0,z') + K_1K\Phi(x_0,z')\right] \cdot G(x,x_0,z,z')dz' \\ &\quad + \int_{z_1}^{z_2}\left[(\mu-1)\Phi_x(a-x_0,z') + K_1K\Phi(a-x_0,z')\right] \cdot G(x,a-x_0,z,z')dz'. \end{aligned} \quad (13)$$

Equation (13) represents the most general formulation to the problem of MSW propagation in a normally magnetized waveguide structure.

The integral expression given by (13) is two dimensional and very difficult to analyze. Assuming the slab to be very thin makes this equation one dimensional and tractable. With this assumption and utilizing an effective numerical technique combined with an exact simulation algorithm (see Appendix A), the final resolution of the problem can successfully be obtained.

IV. Approximate Solution

As noted in (13), the first term involves a second-order partial derivative term (Φ_{zz}) which must be evaluated properly. To be able to obtain Φ_{zz}, the thin slab is subdivided into two layers of equal thickness, i.e., $z_1 \le z \le z_0$ and $z_0 \le z \le z_2$ (Fig. 1). The variation of $\Phi(x,z)$ in each layer in the z-direction is assumed to be linear. In this manner three functions, each having one variable, are used to approximate $\Phi(x,z)$ in the slab as follows:

$$f_1(x) = \Phi(x,z_1),$$
$$f_0(x) = \Phi(x,z_0),$$
$$f_2(x) = \Phi(x,z_2).$$

The linear approximation gives:

$$\Phi_z(x,z) = \frac{f_0(x) - f_1(x)}{z_0 - z_1}, \qquad z_1 \le z \le z_0. \quad (14a)$$
$$\Phi_z(x,z) = \frac{f_2(x) - f_0(x)}{z_2 - z_0}, \qquad z_0 \le z \le z_2. \quad (14b)$$

and

$$\Phi_{zz}(x,z) = \frac{f_2(x) - 2f_0(x) + f_1(x)}{d^2}, \quad (15)$$

where $d = z_0 - z_1 = z_2 - z_0 = t/2$ and t is the slab thickness.

In the integral equation (13), the second and third terms are surface integrals over the sides of the slab at $x = x_0$ and $a - x_0$. In the thin-slab assumption, instead of a continuous distribution of surface charge in z, the charge distribution on both sides of the slab (x_0 and $a - x_0$) in each region $z_1 \le z \le z_0$ and $z_0 \le z \le z_2$ is assumed to be uniform. This uniform charge distribution assumption connotes that the surface charge in each region is equal to the mean of its values at the edges of that region.

The main reason for uniform charge distribution at the slab sides ($x = x_0$ and $a - x_0$) is the fact that $\Phi(x,z)$ is evaluated only at three values of z, i.e., $z = z_1, z_0$, and z_2. The function $\Phi(x,z)$ between these values is unknown and so all the equations should involve calculations of $\Phi(x,z)$ strictly at these three values of z. The continuous charge distribution would not be a plausible assumption under these conditions.

Substituting for $G(x,x',z,z')$ in (13), carrying out the z-integrals and evaluating the potential function $\Phi(x,z)$ at $z = z_1, z_0$, and z_2 would yield a set of three coupled equations in terms of $f_1(x)$, $f_0(x)$ and $f_2(x)$. By introducing the following functions

$$G_v(x) = f_2(x) - 2f_0(x) + f_1(x) \quad (16)$$
$$G_s(x) = f_2(x) + 2f_0(x) + f_1(x). \quad (17)$$

This set of three coupled equations can be reduced to a set of two coupled equations which is more attractive to work with

$$G_v(x) = -\sum_{n=0}^{\infty} \frac{2W^nQ^n}{a(1+\delta_{on})}\cos n\pi x/a \quad (18a)$$
$$G_s(x) = -\sum_{n=0}^{\infty} \frac{2U^nQ^n}{a(1+\delta_{on})}\cos n\pi x/a \quad (18b)$$

where

$$U^n = V_n\Big[(B_1^n+B_2^n)\cosh\gamma_n'(b-z_2)+(B_3^n+B_4^n)\cosh\gamma_n' z_1 + 2B_1^n\cosh\gamma_n'(b-z_0)+2B_4^n\cosh\gamma_n' z_0\Big], \quad (19)$$

$$W^n = V_n\Big[(B_1^n+B_2^n)\cosh\gamma_n'(b-z_2)+(B_3^n+B_4^n)\cosh\gamma_n' z_1 - 2B_1^n\cosh\gamma_n'(b-z_0)-2B_4^n\cosh\gamma_n' z_0\Big], \quad (20)$$

$$Q^n = \int_{x_0}^{a-x_0}\frac{\mu-1}{\mu d^2}G_v(x)\cos\frac{n\pi}{a}x\,dx - \cos\frac{n\pi}{a}x_0\left(\frac{\mu-1}{4}G_s(x_0)+\frac{K_1K}{4}\frac{dG_s(x_0)}{dx}\right) + \cos\frac{n\pi}{a}(a-x_0)\cdot\left(\frac{\mu-1}{4}G_s(a-x_0)+\frac{K_1K}{4}\frac{dG_s(a-x_0)}{dx}\right), \quad (21)$$

$$V_n = 1/(\gamma_n'\sinh\gamma_n' b),$$

$$B_1^n = \int_{z_1}^{z_0}\cosh\gamma_n' z'\,dz', \quad B_2^n = \int_{z_0}^{z_2}\cosh\gamma_n' z'\,dz',$$

$$B_3^n = \int_{z_1}^{z_0}\cosh\gamma_n'(b-z')dz',$$

$$B_4^n = \int_{z_0}^{z_2}\cosh\gamma_n'(b-z')dz'.$$

The term Q^n in (21) involves the first-order derivative of $G_s(x)$. The function $G_s(x)$ is defined to be nonzero in the YIG and zero everywhere outside, which means it is discontinuous at $x = x_0$ and $x = a - x_0$ and thus its derivatives in the x-direction at the slab edges are undefined. This problem creates difficulty in the evaluation of Q^n. To overcome this problem of discontinuity, the function $G_s(x)$ is defined only in the range $x_0 \le x \le a - x_0$. In this manner, the function $G_s(x)$ becomes differentiable at $x = x_0$ and $a - x_0$ and its approximate finite series expansion can be written as follows:

$$G_s(x) = P_0 + \sum_{L=1}^{N_0} p_L\cos\frac{L\pi}{a-2x_0}(x-x_0) + \sum_{L=1}^{N_0} q_L\sin\frac{L\pi}{a-2x_0}(x-x_0), \quad x_0 \le x \le a-x_0, \quad (22)$$

where p_L's and q_L's are arbitrary constants and N_0 is a very large integer number. Upon differentiation of $G_s(x)$ and use of the series expansion for $G_s(x)$ and dG_s/dx, the expression for Q^n becomes:

$$Q^n = \frac{\mu-1}{\mu d^2}\int_{x_0}^{a-x_0}G_v(x)\cos\frac{n\pi}{a}x\,dx - \cos\frac{n\pi}{a}x_0\left[\frac{\mu-1}{4}\left(p_0+\sum_{L=1}^{N_0}p_L\right) + \frac{KK_1}{4}\sum_{L=1}^{N_0}\frac{L\pi}{a-2x_0}q_L\right] + \cos\frac{n\pi}{a}(a-x_0)\left[\frac{\mu-1}{4}\left(p_0+\sum_{L=1}^{N_0}(-1)^L p_L\right) + \frac{KK_1}{4}\sum_{L=1}^{N_0}(-1)^L\frac{L\pi}{a-2x_0}q_L\right]. \quad (23)$$

Utilizing (23) and further mathematical manipulation, (18) yields the following set of linearly independent equations:

$$C_v^m + \sum_{n=0}^{\infty}\alpha_{mn}Q^nW^n = 0, \quad (24a)$$

$$C_s^m + \sum_{n=0}^{\infty}\alpha_{mn}Q^nU^n = 0, \quad (24b)$$

$$S_s^m + \sum_{n=0}^{\infty}\beta_{mn}Q^nU^n = 0. \quad (24c)$$

where

$$C_v^m = \int_{x_0}^{a-x_0}\cos\left(\frac{m\pi}{a}x\right)G_v(x)dx.$$

$$C_s^m = \int_{x_0}^{a-x_0}\cos\left(\frac{m\pi}{a}x\right)G_v(x)dx$$

$$S_s^m = \int_{x_0}^{a-x_0}\sin\left(\frac{m\pi}{a}x\right)G_v(x)dx$$

$$\alpha_{mn} = \frac{2}{a(1+\delta_{on})}\int_{x_0}^{a-x_0}\cos\left(\frac{m\pi}{a}x\right)\cos\left(\frac{n\pi}{a}x\right)dx,$$

$$\beta_{mn} = \frac{2}{a(1+\delta_{on})}\int_{x_0}^{a-x_0}\sin\left(\frac{m\pi}{a}x\right)\cos\left(\frac{n\pi}{a}x\right)dx,$$

$$m = 0,1,2,\cdots,N_0 \quad \text{and} \quad n = 0,1,2,\cdots,N_0.$$

The term Q^n in (23) is expressed in terms of constant coefficients p_L and $q_L(L = 1,\cdots,N_o)$; however, through a certain procedure it is possible to express them in terms of two of the variables of (24) which are C_s^m and S_s^m as follows:

$$\begin{bmatrix}p_0\\p_1\\\vdots\\p_{N_o}\\q_1\\\vdots\\q_{N_o}\end{bmatrix} = [H]^{-1}\begin{bmatrix}C_s^0\\C_s^1\\\vdots\\C_s^{N_o}\\S_s^1\\\vdots\\S_s^{N_o}\end{bmatrix} \quad (25)$$

where $[H]^{-1}$ is the inverse of a known matrix $[H]$, (see Appendix B).

Substitution of P_L's and q_L's as given by (25) for Q^n in (24) will produce a system of linear equations in C_v^m, C_s^m, and S_s^m. To obtain a nontrivial solution for this solution for this system of linear equations, it is required that the large determinant $(N_o \times N_o)$ of the coefficient matrix to be set to zero. However, for practical purposes the matrix should be properly truncated for best accuracy. The truncation cut-off point of the matrix depends on the mode of propagation.

For example, for the first- and second-order modes minimum matrix sizes were found to be 4×4 and 6×6 respectively. For higher order modes, larger matrices must be considered.

In the next section (24) is discussed in detail for the first-order mode ($m = 1$) and a simulation algorithm and a computer program based on a truncated matrix is developed to provide numerical insight into the problem.

V. Numerical Analysis and Computer Simulation Results

In Section IV, the basic formulation for magnetostatic wave propagation for a normal magnetic bias field was derived and was given by (24). In this section a special case i.e., that of the first-order mode is further analyzed and sample numerical solutions are obtained.

For the first-order mode ($m = 0, 1$ and $n = 0, 1$) (24) is used to derive the dispersion relations. Through further mathematical work for this mode, (24) when cast into a concise matrix notation, becomes

$$[M(f,K)] \cdot \begin{bmatrix} C_v^0 \\ C_v^1 \\ C_s^0 \\ C_s^1 \\ S_s^1 \end{bmatrix} = 0, \tag{26}$$

where $[M(f,k)]$ is shown at the bottom of this page, and where

$$F = \frac{\mu - 1}{\mu d^2},$$

$$D_0 = \left(-\frac{(\mu-1)}{4}(h'_{11} + h'_{21}) - \frac{K^2 K_1 \pi}{4(a-2x_0)} h'_{31}\right) \cos\frac{\pi}{a}x_0 + \left(\frac{(\mu-1)}{4}(h'_{11} - h'_{21}) - \frac{K^2 K_1 \pi}{4(a-2x_0)} h'_{31}\right) \cos\frac{\pi}{a}(a - x_0),$$

$$D_1 = \left(-\frac{(\mu-1)}{4}(h'_{12} + h'_{22}) - \frac{K^2 K_1 \pi}{4(a-2x_0)} h'_{32}\right) \cos\frac{\pi}{a}x_0 + \left(\frac{(\mu-1)}{4}(h'_{12} - h'_{22}) - \frac{K^2 K_1 \pi}{4(a-2x_0)} h'_{32}\right) \cos\frac{\pi}{a}(a - x_0),$$

$$D_2 = \left(-\frac{(\mu-1)}{4}(h'_{13} + h'_{23}) - \frac{K^2 K_1 \pi}{4(a-2x_0)} h'_{33}\right) \cos\frac{\pi}{a}x_0 + \left(\frac{(\mu-1)}{4}(h'_{13} - h'_{23}) - \frac{K^2 K_1 \pi}{4(a-2x_0)} h'_{33}\right) \cos\frac{\pi}{a}(a - x_0),$$

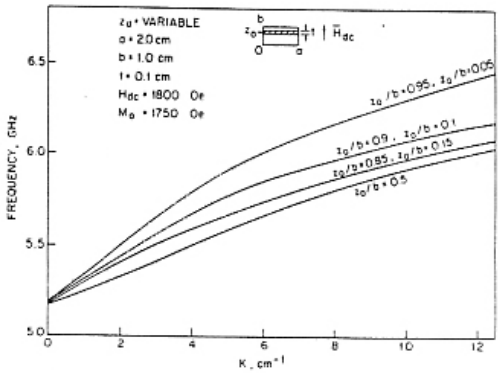

Fig. 2. Dispersion curves for different slab positions.

$$[H]^{-1} = \begin{bmatrix} h'_{11} & h'_{12} & h'_{13} \\ h'_{21} & h'_{22} & h'_{23} \\ h'_{31} & h'_{23} & h'_{33} \end{bmatrix}.$$

It is to be noted that $[H]$ is a known matrix (see Appendix B) which was calculated and wherefrom its corresponding inverted matrix was worked out with the aid of a computer, so that the results of this inversion could be used in (26). Requiring a nontrivial unique solution yields the dispersion relation. This dispersion relation is obtained by setting the determinant of $[M(f,K)]$ to zero. To find the dispersion relation for the first-order mode, the following equation must be solved:

$$|M(f,K)| = 0. \tag{27}$$

With the aid of a proper simulation algorithm, and by employing the Newton–Raphson method the determinant roots of the dispersion relations were found through several iterations (see Appendix A)

Fig. 2 shows the effect of slab position in the waveguide on the dispersion characteristics. From this figure it can be seen that the effect of slab position on the dispersion curve becomes pronounced at the higher frequencies in the propagation band. Although the characteristics all converge at the lower end of the propagation band, their slopes are different. This leads to different group time delays as can be seen in Fig. 3. This figure shows the group time delay corresponding to Fig. 2. It can be observed that as the slab is placed toward the center of the guide, the group time delay increases while the propagation bandwidth decreases.

Width effects on the device performance was also studied and the results are shown in Figs. 4 and 5. In Fig. 4, it can be

$$[M(f,K)] = \begin{bmatrix} 1+F\alpha_{00}W^0 & F\alpha_{01}W^1 & D_0\alpha_{01}W^1 & D_1\alpha_{01}W^1 & D_2\alpha_{01}W^1 \\ F\alpha_{10}W^0 & 1+F\alpha_{11}W^1 & D_0\alpha_{11}W^1 & D_1\alpha_{11}W^1 & D_2\alpha_{11}W^1 \\ F\alpha_{00}U^0 & F\alpha_{01}U^1 & 1+D_0\alpha_{01}U^1 & D_1\alpha_{01}U^1 & D_2\alpha_{01}U^1 \\ F\alpha_{10}U^0 & F\alpha_{11}U^1 & D_0\alpha_{11}U^1 & 1+D_1\alpha_{11}U^1 & D_2\alpha_{11}U^1 \\ F\beta_{10}U^0 & F\beta_{11}U^1 & D_0\beta_{11}U^1 & D_1\beta_{11}U^1 & 1+D_2\beta_{11}U^1 \end{bmatrix}$$

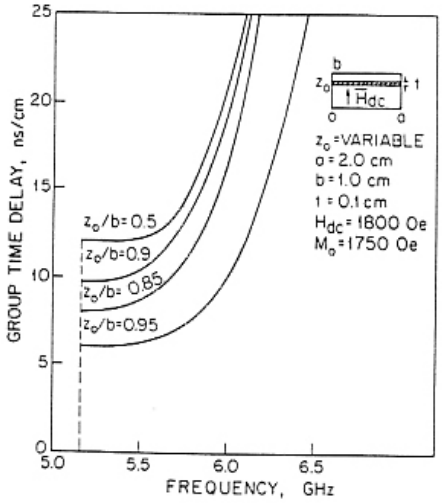

Fig. 3. Time delay versus frequency for different slab positions.

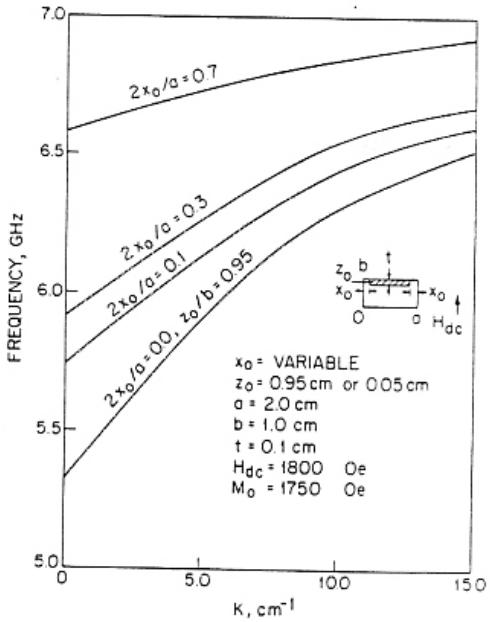

Fig. 4. Dispersion curves for different slab widths.

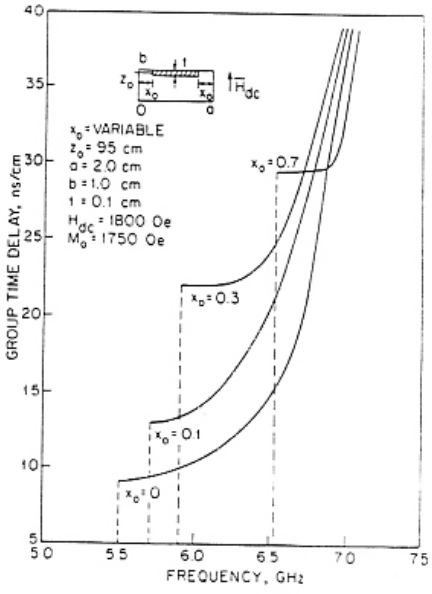

Fig. 5. Time delay versus frequency for different slab widths.

VI. Summary and Conclusion

Magnetostatic wave propagation in a normally magnetized waveguide structure was analyzed and the general solution to the problem with the use of the integral equation method was derived. Thin-slab approximation led to a set of linearly independent equations which provided the dispersion relations in terms of an infinite determinant. Using proper truncation procedures several important effects were studied. The dependence of the dispersion relations and group time delay per unit length on the position and width of the YIG slab and sample numerical solutions for the first-order mode for several configurations over a frequency range of 5.0–7.0 GHz were discussed and the results were presented.

It was also observed that the propagating waves, unlike parallel magnetization case, are reciprocal with respect to the direction of propagation and symmetrical with respect to the slab position in the waveguide.

seen that as the normalized air gap increases the propagation bandwidth decreases and the curves flatten out as they shift toward higher frequencies. Fig. 5 shows the corresponding group time delay versus frequency. From this figure it can be seen that as the slab width decreases (or the air gap increases) the group time delay increases toward higher values with smaller bandwidths as noted earlier. The group time delay at smaller slab widths remains constant in a larger bandwidth and also has a higher value. This property can be used effectively in device design to obtain a constant, high group delay per unit length in a desired frequency band. Fig. 6 plots wave number K versus the normalized air gap $(2x_0/a)$. In this figure, the information of Fig. 4 is rearranged in a different fashion. It can be seen that the wave propagation at small slab widths (or large air gaps) is possible only at higher frequencies with smaller wavelengths (or higher K). Once the slab width is chosen, Fig. 6 shows the frequency at which the device must be operated to obtain a certain wavelength, and vice versa.

As can be observed from these results, the effect of finite sample width is significant in the low-wave number region which is in good agreement with earlier works [9], [10], and [14].

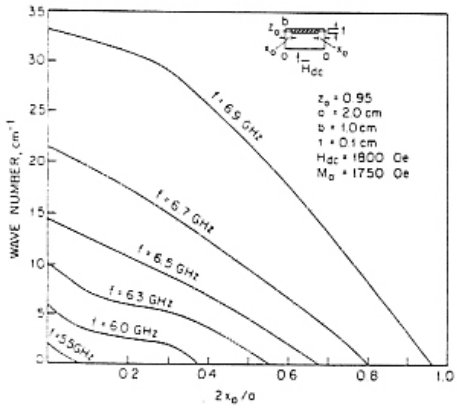

Fig. 6. Wave number (k) versus normalized air gap for different frequencies.

From these observations, it can be concluded that to obtain high values of group time delay over a large bandwidth, very thin slabs are required. To increase the time delay even more, it is best to choose a narrow width slab and place it in the center of the waveguide.

Appendix A
Algorithm for Dispersion Characteristics

The equation to be solved numerically is the dispersion relation, a function of frequency (f) and wave number (k), which can be written as

$$D(f, K) = 0 \tag{A1}$$

where $D(f, K)$ represents the determinant of the coefficient matrix involved in the system of linear equations ($|M(f, K)|$). Equation (A1), in general, is a nonlinear function of f and K and can be quite complicated if the size of the matrix is large.

With the aid of the Newton–Raphson method, (A1) is solved numerically for roots K (at a known frequency f_1). The following algorithm details the exact steps used in programming (A1) in order to find its roots:

Step 1. Input and Definition: Read f_1 = the frequency of operation, K_1 = the initial approximation of the root of:

$$D(f_1, K) = 0$$

ϵ = the convergence term and N = the maximum number of iterations.

Step 2. Initialization: Set iteration counter $i = 1$. Set the correction term

$$\Delta_1 = C_1 \tag{A2}$$

(C_1 is an arbitrary large positive number).

Step 3. Compute successive approximation of root using the Newton–Raphson iterative formula:

$$K_{i+1} = K_i - \frac{D(f_1, K_i)}{D'(f_1, K_i).} \tag{A3}$$

Compute the magnitude of the correction term in the current iteration:

$$\Delta_{i+1} = |K_{i+1} - K_i|. \tag{A4}$$

Step 4. Test for convergence or failure to converge:

1. If $\Delta_{i+1} \leq \epsilon$ and $|D(f_1, K_{i+1})| \leq \epsilon$, go to Step 5. If not continue.
2. If $\Delta_{i+1} > \Delta_i$, select new K_1 and return to Step 2. If $\Delta_{i+1} \leq \Delta_i$ continue.
3. If $i \leq N$, set $i = i + 1$ and return to Step 3. If $i > N$, select new K_i and return to Step 2.

Step 5. Output root K_o: set $K_o = K_{i+1}$. Write K_o.

Appendix B

The coefficient matrix $[H]$ is given by (B1), which is at the bottom of this page, where

$$(CC)_n^m = \int_{x_0}^{a-x_0} \cos\frac{n\pi}{a-2x_0}(x-x_0)\cos\frac{m\pi}{a}x\,dx,$$

$$(CS)_n^m = \int_{x_0}^{a-x_0} \cos\frac{n\pi}{a-2x_0}(x-x_0)\sin\frac{m\pi}{a}x\,dx,$$

$$(SC)_n^m = \int_{x_0}^{a-x_0} \sin\frac{n\pi}{a-2x_0}(x-x_0)\cos\frac{m\pi}{a}x\,dx,$$

$$(SS)_n^m = \int_{x_0}^{a-x_0} \sin\frac{n\pi}{a-2x_0}(x-x_0)\sin\frac{m\pi}{a}x\,dx,$$

and

$$n = 0, 1, 2, \cdots, N_0$$
$$m = 0, 1, 2, \cdots, N_0.$$

$$[H] = \begin{bmatrix} (CC)_0^0 & (\mathrm{CC})_1^0 & (\mathrm{CC})_2^0 & \cdots & (\mathrm{CC})_{N_0}^0 & (\mathrm{SC})_1^0 & (\mathrm{SC})_2^0 & \cdots & (\mathrm{SC})_{N_0}^0 \\ (CC)_0^1 & (\mathrm{CC})_1^1 & (\mathrm{CC})_2^1 & \cdots & (\mathrm{CC})_{N_0}^1 & (\mathrm{SC})_1^1 & (\mathrm{SC})_2^1 & \cdots & (\mathrm{SC})_{N_0}^1 \\ \vdots & & & & \vdots & \vdots & & & \vdots \\ (CC)_0^{N_0} & (\mathrm{CC})_1^{N_0} & (\mathrm{CC})_2^{N_0} & \cdots & (\mathrm{CC})_{N_0}^{N_0} & (\mathrm{SC})_1^{N_0} & (SC)_2^{N_0} & \cdots & (\mathrm{SC})_{N_0}^{N_0} \\ (CS)_0^1 & (\mathrm{CS})_1^1 & (\mathrm{CS})_2^1 & \cdots & (\mathrm{CS})_{N_0}^1 & (\mathrm{SS})_1^1 & (\mathrm{SS})_2^1 & \cdots & (\mathrm{SS})_{N_0}^1 \\ \vdots & & & & \vdots & \vdots & & & \vdots \\ (CS)_0^{N_0} & (\mathrm{CS})_1^{N_0} & (\mathrm{CS})_2^{N_0} & \cdots & (\mathrm{CS})_{N_0}^{N_0} & (\mathrm{SS})_1^{N_0} & (SS)_2^{N_0} & \cdots & (\mathrm{SS})_{N_0}^{N_0} \end{bmatrix} \tag{B1}$$

REFERENCES

[1] I. J. Weinberg, "Dispersion relations for magnetostatic waves," in *1980 IEEE Ultrasonic Symp Proc.*, Boston, pp. 557–561.

[2] M. C. Tsai, H. J. Wu, J. M. Owens, and C. V. Smith, Jr., "Magnetostatic propagation for uniform normally magnetized multilayer planar structure," in *1976 AIP Conf. Proc.* Pittsburgh, no. 34, pp. 280–282.

[3] T. Yukawa, J. Ikenoue, J. Yamada and K. Abe, "Effects of metal on dispersion relations of magnetostatic volume waves," *J. Applied Physics*, vol. 49, pp. 376–382, 1978.

[4] M. R. Daniel, J. D. Adam, and T. W. O'Keefe, "Linearly dispersive delay lines at microwave frequencies using magnetostatic waves," in *Ultrasonic Symp. Proc.*, 1979, pp. 806–809.

[5] K. Yashiro, S. Ohkawa, and M. Miyazaki, "Boundary element method approach to magnetostatic wave problems," *IEEE Trans. Microwave Theory Tech.*, vol. MTT-33, pp. 248–253, May 1985.

[6] B. A. Auld, K. B. Mehta, "Magnetostatic waves in a transversely magnetized rectangular rod," *J. Applied Physics*, vol. 38, no. 10, pp. 4081–4082, Sept. 1967.

[7] M. Radmanesh, C. M. Chu, and G. I. Haddad, "Magnetostatic wave propagation in a yttrium iron garnet (YIG)-loaded waveguide," *Microwave J.*, vol. 29, no. 7, pp. 135–140, July 1986.

[8] ——, "Magnetostatic wave propagation in a finite YIG-loaded rectangular waveguide," *IEEE Trans. Microwave Theory Tech.*, vol. 34, no. 12, pp. 1377–1382, Dec. 1986.

[9] Y. Long, M. Koshiba and M. Suzuki, "Finite element solution of planar in homogeneous waveguides for magnetostatic waves," *IEEE Trans. Microwave Theory Tech.*, vol. MTT-35, pp. 731–736, Aug. 1987.

[10] M. Koshiba, Y. Long, "Finite element analysis of magnetostatic wave propagation in a YIG film of finite dimensions," *IEEE Trans. Microwave Theory and Tech.*, vol. 37, no. 11, Nov. 1989.

[11] M. Radmanesh, C. M. Chu, and G. I. Haddad, "The analysis of magnetostatic waves in a waveguide using the integral equation method," *IEEE MTT-S Int. Microwave Symp. Dig.*, vol. 11, May 1988, pp. 765–768.

[12] ——, "Magnetostatic waves in a normally magnetized waveguide structure," *IEEE Trans. Microwave Theory Tech.*, vol. 35, no. 12, pp. 1226–1230, Dec. 1987.

[13] B. Lax and R. J. Button, *Microwave Ferrites and Ferrimagnetics*. New York: McGraw-Hill, 1962, pp. 297–322.

[14] S. N. Baipai and N. C. Srivastava, "Magnetostatic bulk wave propagation in multilayered structure," *Electron. Lett.*, vol. 16, pp. 269–270, Mar. 1980.

Matthew M. Radmanesh (M'87) received the B.S.E.E. degree from Pahlavi University in 1978, the M.S.E.E. and Ph.D. degrees in microwave electronics and electro-optics from the University of Michigan, Ann Arbor, in 1980 and 1984 respectively.

From 1979 to 1984, he was a research assistant in the Solid-State Electronics Laboratory at the University of Michigan where he worked on IMPATT's, p-i-n diodes, and MESFET amplifier design. In 1984 he joined GMI Engineerings & Management Institute and served as a faculty member until 1987. During this period he was involved in research on microwave devices and circuits, particularly YIG and magnetostatic wave (MSW) devices. From 1987 to 1990 he served as a senior scientist at Hughes Aircraft Company and McDonnell Douglas Corporation. During this period of time he focused his reserch in millimeter wave and microwave active circuits, particularly millimeter wave noise source design as well as millimeter wave measurement and calibration techniques. He was awarded the 1988 Hughes MPD divisional award for outstanding achievement in millimeter wave noise sources and holds two patents in this area. He also received a similar award for his work on HERF and EMC/EMI from McDonnell Douglas Corporation in 1990. He is currently a faculty member at the Department of Electrical and Computer Engineering, California State University, Northridge. His research interests include microwave and millimeter wave devices and circuits as well as integrated optics.

Dr. Radmanesh is a member of Eta Kapa Nu and the American Society for Engineering Education. He has authored and coauthored over twenty technical papers in microwaves, millimeter waves and fiber optics.

Chiao-Min Chu received the Ph.D. degree in electrical engineering from the University of Michigan, Ann Arbor, in 1952.

Since then he has held several appointments on the research staff at the University of Michigan. He joined the electrical engineering faculty as an Assistant Professor in 1956 and was promoted to Full Professor in 1963. He conducts research on electrical transmission, wave propagation, and the scattering of waves by conducting and dielectric particles, including scattering from terrain and the sea. Dr. Chu has conducted research on wave propagation through anisotropic and random media and on the statistical analysis of signals scattered from random surfaces. He is now retired as Professor Emeritus from the Department of Electrical Engineering and Computer Science at the University of Michigan.

George I. Haddad received the B.S.E., M.S.E. and Ph.D. degrees in electrical engineering all from the University of Michigan.

From 1957 to 1958 he was associated with the Engineering Research Institute of the University of Michigan, where he was engaged in research on electromagnetic accelerators. In 1958 he joined the Electron Physics Laboratory. From 1960 to 1969 he served successively as Instructor, Assistant Professor, Associate Professor, and Professor in the Electrical Engineering Department. He served as Director of the Electron Physics Laboratory from 1968 to 1975. From 1975 to 1987, Dr. Haddad served as Chairman of the Department of Electrical Engineering and Computer Science. From 1987 to 1991 he served as the Director of both the Solid-Site Electronics Laboratory and the Center for High-Frequency Microelectronics. Since 1991 he has been serving as Chairman of the Department of Electrical Engineering and Computer Science. His current research areas are microwave and millimeter-wave solid state devices, monolithic integrated circuits and microwave-optical interactions.

Dr. Haddad received the 1970 Curtis W. McGraw Research Award of the American Society for Engineering Education for outstanding achievements by an engineering teacher. He was also the recipient of the College of Engineering Excellence in Research Award (1985) and the Distinguished Faculty Achievement Award (1986) of the University of Michigan. He is a member of Eta Kappa Nu, Sigma Xi, Phi Kappa Phi, Tau Beta Pi, and the American Society for Egineering Education, and has published over 200 technical papers on many aspects of microwve and optoelectronic engineering.